

1 **Experimental evidence for lava-like mud flows under Martian surface conditions**

2 Petr Brož<sup>1\*</sup>, Ondřej Krýza<sup>1</sup>, Lionel Wilson<sup>2</sup>, Susan J. Conway<sup>3</sup>, Ernst Hauber<sup>4</sup>, Adriano  
3 Mazzini<sup>5</sup>, Jan Raack<sup>6</sup>, Matthew R. Balme<sup>7</sup>, Matthew E. Sylvest<sup>7</sup> and Manish R. Patel<sup>7,8</sup>

4 <sup>1</sup>Institute of Geophysics of the Czech Academy of Sciences, Boční II/1401, 141 31, Prague,  
5 Czech Republic

6 <sup>2</sup> Lancaster Environment Centre, Lancaster University, Lancaster LA1 4YQ, UK

7 <sup>3</sup> CNRS UMR-6112 LPG Nantes, France

8 <sup>4</sup>Institute of Planetary Research, DLR, Rutherfordstr. 2, 12489, Berlin, Germany

9 <sup>5</sup>Centre for Earth Evolution and Dynamics (CEED), University of Oslo, Norway

10 <sup>6</sup>Institut für Planetologie, Westfälische Wilhelms-Universität Münster, Germany

11 <sup>7</sup>School of Physical Science, STEM, The Open University, Milton Keynes, UK Open  
12 University, Milton Keynes, United Kingdom

13 <sup>8</sup>Space Science and Technology Department, STFC Rutherford Appleton Laboratory, Oxford,  
14 UK

15 *Corresponding Author*

16 Petr Brož

17 Institute of Geophysics of the Czech Academy of Sciences

18 Boční II/1401

19 14131 Prague 4

20 Czech Republic

21 [Petr.broz@ig.cas.cz](mailto:Petr.broz@ig.cas.cz)

22 +420267103063

23

24 Nature Geoscience, <https://doi.org/10.1038/s41561-020-0577-2>

25

26        **Large outflow channels on ancient terrains of Mars have been interpreted as the**  
27 **products of catastrophic flood events. The rapid burial of water-rich sediments**  
28 **following such flooding could have led to sedimentary volcanism, in which mixtures of**  
29 **sediment and water (mud) erupt to the surface. Tens of thousands of volcano-like**  
30 **landforms populate the northern lowlands and other local sedimentary depocenters on**  
31 **Mars. However, it is difficult to determine whether the edifices are related to igneous**  
32 **or mud extrusions, partly because the behaviour of extruded mud under martian**  
33 **surface conditions is poorly constrained. Here, we investigate the mechanisms of mud**  
34 **propagation on Mars using experiments performed inside a low-pressure chamber at**  
35 **cold temperatures. We find that low viscosity mud under martian conditions**  
36 **propagates differently from on Earth, because of rapid freezing and the formation of**  
37 **an icy crust. Instead, the experimental mud flows propagate like terrestrial pahoehoe**  
38 **lava flows, with liquid mud spilling from ruptures in the frozen crust, then refreezing**  
39 **to form a new flow lobe. We suggest that mud volcanism can explain the formation of**  
40 **some lava-like flow morphologies on Mars, and that similar processes may apply to**  
41 **cryovolcanic extrusions on icy bodies in the Solar System.**

42        The physics behind igneous volcanism on Mars is better understood [e.g., 1-4] than that  
43 of sedimentary volcanism in which mixtures of water and sediment, subsequently referred  
44 to as mud, are extruded onto the surface. On Earth, sedimentary volcanism manifests at the  
45 surface as eruptions of fluids (water, gas, occasionally oil), fine grained sediments (e.g.  
46 clays) and clasts from the country-rock. These geological phenomena are the result of fluid  
47 (on Earth typically associated with methane) overpressure [5], generated at several hundred  
48 to several thousand metres depth, combined with gravitational instability of buoyant  
49 sedimentary units buried at deeper stratigraphic levels [6]. The viscosity of ascending mud  
50 varies, and affects the shapes, sizes and thicknesses of resulting flows. The higher the water

51 content, the lower the viscosity and vice versa (Figure 1). The focus of our experimental  
52 investigation are water-dominated mud flows that propagate over shallow slopes via  
53 centimetre-thick flows (Fig. 1a,b), as opposed to clay-dominated flows that can be meter(s)  
54 thick (Fig. 1c).

55 Although the propagation of water at low atmospheric pressure has been previously  
56 studied [7-11], there is a lack of theoretical and empirical knowledge about the behaviour of  
57 mud at low atmospheric pressure, temperature and gravity, despite an initial study by [12].  
58 This knowledge gap represents an obstacle in the study of landforms interpreted to be the  
59 result of mud extrusion on Mars [13-24] and other terrestrial or icy solar system bodies.  
60 Currently, the low martian atmospheric pressure inhibits the sustained presence of liquid  
61 water on the surface [e.g., 7-11,25,26], so evaporation and ice-formation cause the rheology  
62 of the extruded mud to change rapidly; hence mud flows could propagate differently from  
63 on Earth [17].

64 We used analogue experiments performed in a low pressure chamber to examine how low  
65 viscosity, water-dominated mud with a solid fraction of less than ~6.5 wt.% (12.7 mPa.s at  
66 276 K and 10.7 mPa.s at 296 K) propagates over a cold surface (244 K to 265 K) under  
67 terrestrial and martian (7 mbar) atmospheric pressures. These experiments enabled  
68 comparing flow mechanisms at different pressures to be compared and reveal a unique  
69 propagation behaviours under martian conditions. Based on these observations we propose  
70 that evaporation and surficial freezing would dominate the morphology for relatively thin  
71 mud flows (< 1 m) and may influence thicker mud flows hypothesized to be present on the  
72 martian surface [e.g. 12,15,17,24,25].

### 73 **Mud flow experiments**

74 We performed 21 experiments (Table S1 and Fig. S1 in Supplementary Information)  
75 using the Open University (UK) Mars Chamber. During each experiment, 500 ml of mud  
76 was poured over a  $0.9 \times 0.4$  m aluminium tray containing either (a) a  $\sim 2$  cm deep sand bed  
77 ( $\sim 63$ – $200$   $\mu\text{m}$  grain diameter; 14 experiments) representing a sedimentary surface, or (b) a  
78 plastic plate (7 experiments) representing an impermeable icy surface. Fifteen experiments  
79 were performed at  $7 \pm 0.5$  mbar and six experiments at  $\sim 1$  bar (Table S1). The mud was  
80 released onto the surface from a tilting container situated inside the chamber. This design  
81 was chosen for its simplicity and reproducibility, although it represents a simplification of  
82 the natural setting. At the beginning of the experiment the mud was above the freezing point  
83 of water. The temperatures of the sand bed or plastic plate ranged from  $\sim 244$  K to 265 K and  
84 gradually increased with time as no active cooling of the experiment was performed. The  
85 aluminium tray was inclined at  $5^\circ$  (18 experiments) or  $10^\circ$  (3 experiments) to force the mud  
86 to move in a preferred direction. Each experimental run was performed at least in triplicate  
87 and was recorded with four cameras. The experiments did not account for the effect of the  
88 lower gravity on Mars as compared to Earth.

89 At the beginning of each experiment the atmospheric pressure was gradually reduced,  
90 triggering the boiling of the water in the mud [25,27,28]. The mud within the container  
91 cooled by evaporation [25] to almost its freezing point before being poured onto the surface  
92 at a pressure of  $7 \pm 0.5$  mbar (Table S1). Once in contact with the cold surface, the mud  
93 rapidly began to freeze at the bottom and margins of the flow, and at its upper surface (Fig. 2a  
94 and Supplementary Information). The freezing resulted in the formation of an ice-mud crust  
95 which modified flow propagation and decreased lateral spreading (Fig. 3).

96 Mud propagation occurred through an intricate system of narrow flow lobes (Fig. 3b) or  
97 several lobate flows (Fig. 3c and 3d). Their formation was controlled by the development of  
98 frozen marginal ridges that confined the flow of liquid mud inside a central channel. As

99 freezing continued, ice crystals floated to the surface and started to merge. However, mud  
100 still propagated within the crust via a network of “mud tubes”, in an analogous way to flow  
101 within lava tubes (Fig. 2c). When new pulses of mud arrived, they caused breakouts and the  
102 formation of further lobes (Fig. 2b). The newly extruded material rapidly developed a frozen  
103 crust.

104 The presence of internal mud tubes was confirmed by sectioning the frozen mud flows  
105 after the re-pressurization of the chamber. A liquid mud core was present even in the  
106 experiments where mud was exposed to low pressure for several tens of minutes (Fig. 2d,e).  
107 Vesicles ranging in size from 1 to 10 mm were observed within the crusts (Fig. 2d), produced  
108 by vapour bubbles that did not escape. The vesicular nature of the crust inhibited the  
109 conduction of heat [29] from the interior of the flow, increasing the depth to which vapour  
110 bubble nucleation occurred.

### 111 **Comparison with terrestrial lava flows**

112 During flow formation, newly supplied mud was observed to increase the thickness of  
113 lobes up to several centimetres (Fig. 3d) via lifting of the protective crust. This occurred  
114 when the terminal part of the flow was frozen and the mud release was blocked, but newly  
115 supplied mud was still intruding the lobe via mud tubes. This created overpressure within  
116 the mud which was able to lift the crust of the lobes. Once a sufficient volume of mud had  
117 accumulated within the lobe, the overpressure was able to break the crust and a new lobe  
118 formed at the terminus. The mud flow inflated in a manner directly analogous to that of  
119 pahoehoe lava flows [30]. This inflation was observed on 5° and 10° slopes, and for  
120 impermeable and permeable substrates. Under terrestrial atmospheric conditions (i.e. room  
121 pressure and temperature) a mud flow moving over a cold surface did not form lobes, did  
122 not inflate, and had no icy crust (Fig. 3d) regardless of the temperature of the mud (~274,  
123 ~290, and ~293 K were tested). Instead, the mud spread out over the surface in a broad sheet

124 only a few millimetres thick, and was in the liquid phase over the entire length of the flow  
125 (Fig. 3a,d). Only minor freezing was observed in the form of ice crystals on the margins of  
126 the flow after several minutes.

127 Like basaltic lavas on Earth, low viscosity mud flows produce laterally extensive  
128 structures with lower relief than those resulting from high viscosity flows [6]. Because the  
129 mud used in our experiments is water-dominated, it initially behaves as a Newtonian fluid.  
130 In the low-pressure environment, evaporative cooling leads to the formation of ice crystals,  
131 which increase the solid content forming a protective crust. The mud evolves into a non-  
132 Newtonian fluid with non-zero yield strength as the total solid volume fraction increased  
133 beyond ~15% [31]. This behaviour is similar to that of low viscosity basaltic lavas whose  
134 movement is affected by the formation of an external crust, formed by solidification of the  
135 lava due to cooling [32]. In both cases the strength of the visco-elastic part of the crust,  
136 between the brittle outer part and the more fluid interior [30], is able to inhibit lateral  
137 spreading and allows fluid accumulation and vertical inflation.

138 Over time, the water in the flow (i.e. not lost by evaporation) freezes to form ice in the  
139 crust, and hence, the thin crust develops an ever-increasing yield strength due to the ice  
140 crystal network becoming increasingly interconnected between the clay particles (see  
141 rheology references in [33]). This creates a solid with mechanical strength similar to how  
142 mineral crystal frameworks in a cooling silicate rock magma replace the rheological yield  
143 strength of the lava. Thus the strength of the crust increases with time, and more inflation  
144 should occur before breakouts occur, in agreement with our observation of more inflation in  
145 the distal parts of the experimental flows. There is no reason to assume that the mechanical  
146 strength of the crust would be different on Mars for mud with the same clay content. Since  
147 the rate, as well as the mode, of its formation are controlled by the non-equilibrium  
148 thermodynamics of vapour loss, specifically the transfer of sensible heat to latent heat in the

149 liquid surrounding each nucleating vapour bubble [25], the time-scale of crust development  
150 should also be the same on Mars. Calculations describing these processes are reported in the  
151 Supplementary Information.

152 The above arguments assume that, as in the experiments, the motion of the mud is laminar.  
153 However, it is likely that in large flows, that the fluid motion is turbulent. For steady, uniform  
154 laminar flows of mud with viscosities of 0.01, 0.1, 1 and 10 Pa.s on 0.6° slopes under martian  
155 gravity, the transition to turbulence will occur for mud flows with thicknesses of 17 mm,  
156 8 cm, 36 cm and 1.7 m, respectively (see equations in [12]). As the solid content (silicate  
157 particles and ice crystals) of the mud increases, its viscosity increases, but even for a total  
158 solids content of 60% [e.g. 34] the viscosity does not exceed 1 Pa.s. Thus any low viscosity  
159 mud flow thicker than a few tens of centimetres on Mars will probably be turbulent and we  
160 discuss the applicability of our experiments to this case below.

### 161 **Implications for mud flows on planetary surfaces**

162 In a model of mud flow dynamics on Mars, [12] considered the effect of high solid content  
163 on the non-Newtonian rheology of mud, assuming the rheological properties were constant  
164 everywhere along the flow. Our experiments underline the importance of considering the  
165 thermodynamics of the processes that occur when mud is exposed to the martian  
166 environment. In a turbulent mud flow, mud from all depths will be exposed to the low  
167 atmospheric pressure and will boil, lose vapour, and cool. Thus, it will cool rapidly,  
168 increasing the ice crystal content and evolving a yield strength. As the yield strength  
169 increases, the critical Reynolds number required to sustain turbulence increases [35], but the  
170 associated increase in viscosity causes the actual Reynolds number to decrease. When the  
171 two become equal this forces a transition to laminar flow, encouraging the formation of lobes  
172 and breakouts, as observed in our experiments.

173 Although our small-scale experimental mudflows show characteristics similar to those of  
174 low-viscosity lava flows, they have a different heat loss mechanism. For lava flows simulated  
175 in the laboratory using wax [e.g., 36-37] a modified Péclet number has been used to  
176 distinguish flows that do or do not readily form crusts. This is not appropriate for our flows,  
177 where the heat loss mechanism is decompressional boiling, not conduction and convection  
178 into the environment (for details see Supplementary Information).

179 On Earth, low effusion rates and volumes can lead to the formation of mud flows  
180 (Fig. 1a,b) with similar magnitudes to those in our experiments. Therefore, such terrestrial  
181 flows exported to Mars would be strongly affected by the mechanisms observed in our  
182 experiments. We expect these mechanisms to also be important at the margins of kilometre-  
183 scale flows where their thicknesses decreases and numerous overlapping centimetre-thick  
184 flows occur. Once mud is extruded into the martian surface pressure environment, it would  
185 cool due to evaporative cooling (Fig. 4a) and freezing of the flow surface would eventually  
186 cause a change in the flow regime. From that point, the mud would no longer propagate via  
187 open channel(s) (Fig. 4b), but instead via mud tube(s) (Fig. 4c) and lobes (Fig. 4d). The  
188 distance such a transition occurs from the source would depend on the effusion rates,  
189 volumes, viscosity and temperature of the extruded mud.

190 Our study shows that inflation of decimetre-thick and meter-sized lobes could occur at  
191 the margins of both mud flows and lava flows, thus both igneous and mud volcanism surface  
192 flows could have similar morphological characteristics [e.g., 12,17]. Our calculations show  
193 that the morphologies of mud flows at scales larger than those covered by our experiments  
194 could be affected by the same processes, particularly at their margins. Hence, as their  
195 mechanisms of mud propagation would differ, martian mud volcanoes may be substantially  
196 different in shape from terrestrial ones [17].



197 Sedimentary volcanism has also been proposed for the dwarf planet Ceres [38,39], which  
198 may have a water-muddy ocean beneath a crust made of clays, salts, clathrates and ice  
199 [39,40]. The process of evaporative cooling and associated freezing should also occur there,  
200 affecting the morphologies of resulting effusive landforms; even more so on Ceres than on  
201 Mars as Ceres lacks an atmosphere. The same principles would apply to other Solar System  
202 bodies and icy moons, and so our experimental results should be considered when  
203 interpreting effusive cryovolcanic surface features on these bodies [e.g., 41,42]. Our results  
204 show that it is vital to consider the effects of the differing environmental conditions on other  
205 planetary surfaces when comparing analogue landforms observed on Earth with apparently  
206 similar effusive morphologies on other bodies.

## 207 **References**

- 208 [1] Wilson, L., & Head, J. W. Mars: Review and analysis of volcanic eruption theory and  
209 relationships to observed landforms. *Reviews of Geophysics* 32(3), 221–263 (1994).  
210 <https://doi.org/10.1029/94RG01113>
- 211 [2] Brož, P., Čadek, O., Hauber, E., & Rossi, A. P. Scoria cones on Mars: Detailed investigation  
212 of morphometry based on high-resolution digital elevation models. *Journal of*  
213 *Geophysical Research: Planets* 120, 1512–1527 (2015).  
214 <https://doi.org/10.1002/2015JE004873>
- 215 [3] Parfitt, E. A., & Wilson L. *Fundamentals of Physical Volcanology* (Blackwell, Oxford, U.  
216 K., 2008). ISBN: 978-0-632-05443-5
- 217 [4] Fagents, S. A, Gregg, T. K. P., & Lopes, R. M. C. *Modelling volcanic processes: the physics*  
218 *and mathematics of volcanism* (Cambridge University Press, Cambridge, 2013). ISBN:  
219 9781139021562

- 220 [5] Dimitrov, L. I. Mud volcanoes—the most important pathway for degassing deeply buried  
221 sediments. *Earth-Science Reviews* 59, 1–4, 49–76 (2002). [https://doi.org/10.1016/S0012-](https://doi.org/10.1016/S0012-8252(02)00069-7)  
222 8252(02)00069-7
- 223 [6] Mazzini, A., & Etiope, G. Mud volcanism: An updated review. *Earth-Science Reviews* 168,  
224 81–112 (2017). <https://doi.org/10.1016/j.earscirev.2017.03.001>
- 225 [7] Wallace, D., & Sagan, C. Evaporation of ice in planetary atmospheres: Ice-covered rivers  
226 on Mars. *Icarus* 39, 385–400 (1979). [https://doi.org/10.1016/0019-1035\(79\)90148-9](https://doi.org/10.1016/0019-1035(79)90148-9)
- 227 [8] Carr, M. H. Stability of streams and lakes on Mars. *Icarus* 56, 476–495 (1983).  
228 [https://doi.org/10.1016/0019-1035\(83\)90168-9](https://doi.org/10.1016/0019-1035(83)90168-9)
- 229 [9] Baker, V. R. Erosional processes in channelized water flows on Mars. *Journal of*  
230 *Geophysical Research* 84, 7985–7993 (1979). <https://doi.org/10.1029/JB084iB14p07985>
- 231 [10] Brass, G.W. The stability of brines on Mars. *Icarus* 42, 20–28 (1980).  
232 [https://doi.org/10.1016/0019-1035\(80\)90237-7](https://doi.org/10.1016/0019-1035(80)90237-7)
- 233 [11] Kossacki, K. J., Markiewicz, W. J., Smith, M. D., Page, D., & Murray, J. Possible remnants  
234 of a frozen mud lake in southern Elysium, Mars. *Icarus* 181, 363–374 (2006).  
235 <https://doi.org/10.1016/j.icarus.2005.11.018>
- 236 [12] Wilson, L., & Mougini-Mark, P. J. Dynamics of a fluid flow on Mars: Lava or mud?  
237 *Icarus* 233, 268–280 (2014). <https://doi.org/10.1016/j.icarus.2014.01.041>
- 238 [13] Oehler, D.Z. & Allen, C.C. Evidence for pervasive mud volcanism in Acidalia Planitia,  
239 Mars. *Icarus* 208, 636–657 (2010). <https://doi.org/10.1016/j.icarus.2010.03.031>
- 240 [14] Allen, C.C. et al. Fluid expulsion in terrestrial sedimentary basins: a process providing  
241 potential analogs for giant polygons and mounds in the martian lowlands. *Icarus* 224,  
242 424–432 (2013). <https://doi.org/10.1016/j.icarus.2012.09.018>

- 243 [15] Komatsu, G. et al. Small edifice features in Chryse Planitia, Mars: Assessment of a mud  
244 volcano hypothesis. *Icarus* 268, 56–75 (2016).  
245 <https://doi.org/10.1016/j.icarus.2015.12.032>
- 246 [16] Hemmi, R., & Miyamoto, H. High-resolution topographic analyses of mounds in southern  
247 Acidalia Planitia, Mars: Implications for possible mud volcanism in submarine and  
248 subaerial environments. *Geosciences*, 8(5), 152, 1–19 (2018).  
249 <https://doi.org/10.3390/geosciences8050152>
- 250 [17] Brož, P., Hauber, E., van de Burgt, I., Špillar, V., & Michael, G. Subsurface sediment  
251 mobilization in the southern Chryse Planitia on Mars. *Journal of Geophysical Research:*  
252 *Planets* 124, 703–720 (2019). <https://doi.org/10.1029/2018JE005868>
- 253 [18] Okubo, C. H. Morphologic evidence of subsurface sediment mobilization and mud  
254 volcanism in candor and Coprates Chasmata, Valles Marineris, Mars. *Icarus* 269, 23–37  
255 (2016). <https://doi.org/10.1016/j.icarus.2015.12.051>
- 256 [19] Skinner, J. A., & Mazzini, A. Martian mud volcanism: Terrestrial analogs and implications  
257 for formational scenarios. *Marine and Petroleum Geology* 26(9), 1866–1878 (2009).  
258 <https://doi.org/10.1016/j.marpetgeo.2009.02.006>
- 259 [20] Hemmi, R. & Miyamoto, H. Distribution, morphology, and morphometry of circular  
260 mounds in the elongated basin of northern terra sirenum, mars. *Progress in Earth and*  
261 *Planetary Science* 4, 26, 1–15 (2017). <https://doi.org/10.1186/s40645-017-0141-x>
- 262 [21] Kumar, P. S. et al. Recent seismicity in Valles Marineris, Mars: Insights from young faults,  
263 landslides, boulder falls and possible mud volcanoes, *Earth and Planetary Science Letters*  
264 505, 51–64 (2019). <https://doi.org/10.1016/j.epsl.2018.10.008>

- 265 [22] Brož, P., & Hauber, E. Hydrovolcanic tuff rings and cones as indicators for  
266 phreatomagmatic explosive eruptions on Mars. *Journal of Geophysical Research: Planets*  
267 118, 1656–1675 (2013). <https://doi.org/10.1002/jgre.20120>
- 268 [23] Brož, P., Hauber, E., Wray, J. J., & Michael, G. Amazonian volcanism inside Valles  
269 Marineris on Mars. *Earth and Planetary Science Letters* 473, 122–130 (2017).  
270 <https://doi.org/10.1016/j.epsl.2017.06.003>
- 271 [24] Skinner, J. A., & Tanaka, K. L. Evidence for and implications of sedimentary diapirism  
272 and mud volcanism in the southern Utopia highland-lowland boundary plain, Mars. *Icarus*  
273 186(1), 41–59 (2007). <https://doi.org/10.1016/j.icarus.2006.08.013>
- 274 [25] Bargery, A. S., Lane, S. J., Barrett, A., Wilson, L., & Gilbert, J. S. The initial responses of  
275 hot liquid water released under low atmospheric pressures: Experimental insights. *Icarus*  
276 210(1), 488–506 (2010). <https://doi.org/10.1016/j.icarus.2010.06.019>
- 277 [26] Hecht, M. H. Metastability of liquid water on Mars. *Icarus* 156(2), 373–386 (2002).  
278 <https://doi.org/10.1006/icar.2001.6794>
- 279 [27] Raack, J. et al. Water-induced sediment levitation enhances downslope transport on Mars.  
280 *Nature Communications* 8, 1–10 (2017). <https://doi.org/10.1038/s41467-017-01213-z>
- 281 [28] Herny, C. et al. Downslope sediment transport by boiling liquid water under Mars-like  
282 conditions: Experiments and potential implications for Martian gullies. *Geological*  
283 *Society Special Publication* 467, 373–410 (2019). <https://doi.org/10.1144/SP467.10>
- 284 [29] Smith, D. et al. Thermal conductivity of porous materials. *Journal of Materials Research*  
285 28(17), 2260–2272 (2013). <https://doi.org/10.1557/jmr.2013.179>
- 286 [30] Hon, K., Kauahikaua, J., Denlinger, R., & Mackay, K. Emplacement and inflation of  
287 pahoehoe sheet flows: observation and measurements of active lava flows on Kilauea

- 288 Volcano, Hawaii. *Geological Society of America Bulletin* 106, 351–370 (1994).  
289 [https://doi.org/10.1130/0016-7606\(1994\)106<0351:EAIOPS>2.3.CO;2](https://doi.org/10.1130/0016-7606(1994)106<0351:EAIOPS>2.3.CO;2)
- 290 [31] Ayel, V., Lottin, O., & Peerhossaini, H. Rheology, flow behaviour and heat transfer of ice  
291 slurries: a review of the state of the art. *International Journal of Refrigeration* 26, 95–107  
292 (2003). [https://doi.org/10.1016/S0140-7007\(02\)00016-6](https://doi.org/10.1016/S0140-7007(02)00016-6)
- 293 [32] Cashman, K. V., Kerr, R. C., & Griffiths, R. W. A laboratory model of surface crust  
294 formation and disruption on lava flows through non-uniform channels. *Bulletin of*  
295 *Volcanology* 68(7-8), 753–770 (2006). <https://doi.org/10.1007/s00445-005-0048-z>
- 296 [33] Chevrel M. O., Baratoux, D., Hess, K.-U., & Dingwell, D. B. Viscous flow behavior of  
297 tholeiitic and alkaline Fe-rich martian basalts. *Geochimica et Cosmochimica Acta* 124,  
298 348–365 (2014). <https://doi.org/10.1016/j.gca.2013.08.026>
- 299 [34] Kaitna, R., Rickenmann, D. & Schatzmann, M., Experimental study on rheologic  
300 behaviour of debris flow material. *Acta Geotechnica* 2, 71–85 (2007).  
301 <https://doi.org/10.1007/s11440-007-0026-z>
- 302 [35] Skelland, A.H.P. *Non-Newtonian flow and heat transfer*. (John Wiley and Sons, New  
303 York, 1967).
- 304 [36] Rader, E., Vanderkluisen, L., & Clarke, A. The role of unsteady effusion rates on  
305 inflation in long-lived lava flow fields. *Earth and Planetary Science Letters* 477, 73–  
306 83 (2017). <https://doi.org/10.1016/j.epsl.2017.08.016>
- 307 [37] Fink, J. H., & Griffiths, R. W. A laboratory analog study of the morphology of lava  
308 flows extruded from point and line sources. *Journal of Volcanology and Geothermal*  
309 *Research* 54, 19–32 (1992). [https://doi.org/10.1016/0377-0273\(92\)90112-Q](https://doi.org/10.1016/0377-0273(92)90112-Q)

- 310 [38] Sori, M. M. et al. The vanishing cryovolcanoes of Ceres. *Geophysical Research Letters* 44,  
311 1243–1250 (2017). <https://doi.org/10.1002/2016GL072319>
- 312 [39] Ruesch, O. et al. Slurry extrusion on Ceres from a convective mud-bearing mantle. *Nature*  
313 *Geoscience* 12, 505–509 (2019). <https://doi.org/10.1038/s41561-019-0378-7>.
- 314 [40] Marchi, S. et al. An aqueously altered carbon-rich Ceres. *Nature Astronomy* 3, 140–145  
315 (2018). <https://doi.org/10.1038/s41550-018-0656-0>.
- 316 [41] Allison, M. L. & Clifford, S. M. Ice-covered water volcanism on Ganymede. *Journal of*  
317 *Geophysical Research* 92, 7865–7876 (1987). <https://doi.org/10.1029/JB092iB08p07865>
- 318 [42] Fagents, S.A. Considerations for effusive cryovolcanism on Europa: The post-Galileo  
319 perspective. *Journal of Geophysical Research: Planets* 108 (E12), 5139 (2003).  
320 <https://doi.org/10.1029/2003JE002128>

## 321 **Acknowledgements**

322 The access to the Mars Chamber at the Open University was provided by Europlanet 2020  
323 RI which has received funding from the European Union's Horizon 2020 research and  
324 innovation program under grant agreement No 654208. OK was supported by Center for  
325 Geosphere Dynamics (Faculty of Science at Charles University) project UNCE/SCI/006. LW  
326 was supported by the Leverhulme Trust through an Emeritus Fellowship. AM received funds  
327 from the European Research Council under the European Union's Seventh Framework  
328 Programme Grant agreement n° 308126 (LUSI LAB project, PI A. Mazzini) and acknowledges  
329 the support from the Research Council of Norway through its Centres of Excellence funding  
330 scheme, Project Number 223272 (CEED). The authors thank Steve Lane and Ondřej Čadek for  
331 valuable discussions, Rudolf Koranda from Keramost Company for providing the clay samples,  
332 and to Laszlo Keszthelyi and Alison Graettinger for their constructive comments and insightful  
333 suggestions, which significantly improved this manuscript.

334 **Author contribution**

335 The experimental set-up and the methodology were conceived and designed by P.B. and O.K.  
336 with the help and advice of S.J.C., J.R., M.R.P., M.R.B., A.M., and E.H. The technical support  
337 was provided by M.R.S. The data analysis was done by P.B. with significant feedback from  
338 O.K., L.W., S.J.C., E.H. and A.M. The DEM production was done by O.K. and the theoretical  
339 considerations associated with scaling were done by L.W. All authors contributed to discussion,  
340 interpretation and writing of the manuscript.

341 **Competing interests**

342 The authors declare no competing interests.

343 **Figure captions**

344 **Fig. 1. Examples of surface expressions of terrestrial sedimentary volcanism caused by**  
345 **muds of various viscosity.** (a) A water-dominated mud flowing from the crater of Bakhar mud  
346 volcano in Azerbaijan (39°59'55.7"N, 49°28'29.9"E). (b) An individual mud flow from a  
347 'gryphon' on top of Dashgil volcano in Azerbaijan (39°59'48"N, 49°24'11"E). (b). (c) A  
348 kilometre-sized highly-viscous mud flow outgoing from Koturdag mud volcano in Azerbaijan  
349 (39°58'30"N, 49°21'36"E). Note minibus for scale.

350 **Fig. 2. Examples of morphologies and interior structures of mud flows formed in a low-**  
351 **pressure environment.** Panel **a** shows three frames from video taken by Cam #2 covering  
352 experiment #16 in which the formation of a narrow, thick mud flow occurred. Panel **b** shows in  
353 detail the formation of the icy crust and outbreaks of new mud pulses from beneath the icy-  
354 muddy crust. When the resulting mud flow features were sectioned, large cavities filled with  
355 liquid mud (**c**), or voids (**d**) in the ice were observed. A liquid mud core was commonly  
356 observed in the flow interior (**e**).

357 Fig. 3. **Timeline maps of modelled mud flows derived from the videos and final**  
358 **topographic cross sections.** Flows formed in terrestrial (a) and low-pressure environments  
359 when mud was poured by high (b) or low (c) release rates. The numbered bold lines represent  
360 the margins of the flows at 5 s intervals, the other lines are 1 s intervals. (d) The position of  
361 each topographic profile is marked in panels a, b and c. Topography was measured after the  
362 chamber was re-pressurized.

363 Fig. 4. **Hypothesised development of a low viscosity mud flow on Mars.** (a) The mud  
364 boils and self-cools through evaporative cooling. Once a mud flow develops, the mud is  
365 transported via an open channel (b) evolving into a mud tube due to freezing of the flow surface  
366 (c). The mud propagates via mud tubes to the flow front. As the crust prevents free movement  
367 of the mud, it spreads via lobe breakout (d) which occurs when the pressure inside the frozen  
368 flow is large enough to break the crust or to lift it up; exposing the mud again to the martian  
369 environment.

## 370 **Methods**

371 **Experimental setup.** The low viscosity mud used in our experiments was a mixture of water  
372 that contains 0.5 % w/w dissolved magnesium sulphate ( $\text{MgSO}_4$ ) salts corresponding to the  
373 average river water salinity and clay obtained from the claystone named after the Rokle locality  
374 operated by the company Keramost, which is situated near the town of Kadaň in the Czech  
375 Republic. The clay was a bentonite composed of 76 % montmorillonite, 23 % illite, and 1 %  
376 kaolinite which has been formed by alteration of pyroclastic rocks. As there is no direct in-situ  
377 knowledge of which types of clays could be present on Mars during subsurface sediment  
378 mobilization and as explosive volcanism was once present on Mars [42], to the first  
379 approximation this material seems to be a suitable analogue. To exclude the presence of  
380 potentially more lithified clayey aggregates, the clay was mixed with water and salt and  
381 homogenized in a blender for 3 minutes. Adding the small amount of the salt was necessary to



382 allow submillimetre particles to get into suspension within the mixture [43] and also realistic  
383 for the martian surface [e.g., 44-46]. The resulting viscosity of the mud was 12.7 mPa.s at ~276  
384 K and 10.7 mPa.s at ~296 K and the average density of the mixture was 1037.5 kg.m<sup>-3</sup>. The  
385 viscosity was measured with Haake Rotovisco RV 20 and Viscotester VT 550 rheometers  
386 (Institute of Hydrodynamics of the Czech Academy of Sciences) with ledges on the MV2  
387 cylinder to prevent slip of the measured material on its walls.

388 Each experimental run (for details see Table S1 in the Supplementary Information) started  
389 by inserting the 0.9 × 0.4 m aluminium tray filled with (a) a ~2 cm deep substrate bed (natural  
390 sand, ~200 μm), or b) a plastic plate, and similarly sized copper plate inside the freezer to  
391 pre-cool the tray and the plate to temperatures around 238 K. Once the required temperature  
392 was reached, the plate and the tray were inserted inside the vacuum chamber. At the same  
393 time the 500 ml of liquid mud was poured inside the tilting container equipped with one  
394 thermocouple to record the temperature of the mud, and the container was installed inside  
395 the chamber. The temperature of the mud varied from 274 to 297 K before the pressure drop.  
396 The temperature within the chamber was also monitored by another thermocouple.  
397 Additionally, five thermocouples were set in a grid (see Fig. 1 in the Supplementary  
398 Information for details about the positioning of thermocouples) within the tray in order to  
399 monitor the temperature of the surface over which the mud propagated.

400 Once the tray was in place inside the chamber, a series of images were taken by a single-  
401 lens reflex camera from different angles to obtain the digital elevation model of the pristine  
402 surface before the experimental run. Subsequently the chamber was closed and the process  
403 of depressurization started. To achieve the pressure drop from ambient terrestrial pressure to  
404 7 mbar took usually around 6 minutes. Once the pressure started to drop, the decrease in the  
405 temperature of the mud within the container was measured. Every time the mud self-cooled  
406 close to 273 K during the pressure drop, but it remained liquid. When the pressure of ~7 mbar

407 was reached, the container was manually flipped by the operator and hence mud was poured  
408 from the height of ~5 cm to the surface. The mud flux was not directly measured, we recorded  
409 only the time for how long the mud was extruded (Table S1), as the intense boiling occurred  
410 within the container and hence caused irregularities within the flux.

411 The movement of the mud over the surface was recorded by four video cameras. Once the  
412 mud propagation stopped, the resulting mud flow feature was left in the low pressure  
413 environment for various lengths of time ranging from several minutes to about one hour. After  
414 that the process of re-pressurization of the chamber to terrestrial values started, typically  
415 before temperature of the tray surface rose above ~273 K. Once the pressure inside the chamber  
416 reached atmospheric pressure, the chamber was opened and the resulting flow features were  
417 documented by taking images from different angles to acquire data for subsequent DEM  
418 production. Ultimately the mud flows produced were sectioned and their inner structure was  
419 investigated and documented.

420 **DEM production.** To compare the elevation profiles along and perpendicular to the flow  
421 directions of the mud flows we calculated a series of digital elevation models (DEM). The  
422 sedimentary bed was photographed after each experimental procedure ~30-70 times from  
423 multiple viewpoints. The reconstruction of a 3D model surface was produced by using the  
424 ‘Structure-from-Motion’ [47] commercial software Agisoft PhotoScan. For image orientation  
425 correlation and scaling of the 3D models we used twelve fixed black-on-white printed markers  
426 which were affixed onto flat topped cylindrical posts. The posts had two different elevations  
427 (4.6 cm and 9.6 cm) and the markers were ~2.67 cm in diameter. Typical discrepancies between  
428 actual and calculated marker positions were ~0.8 - 1.6 mm. Exported DEMs and orthophotos  
429 (TIFF format) were imported to QGIS for further analysis and production of the elevation  
430 profiles.

431 **Cooling and freezing of mud when the external pressure is less than the saturation**  
 432 **vapour pressure of the water.** Both the silicate component and the water that has not yet  
 433 vaporized will cool from the initial temperature until the freezing point is reached. After the  
 434 freezing point is reached, the temperature remains constant and vapour continues to be lost until  
 435 all of the remaining water has been converted to ice. If the external pressure is less than the  
 436 saturation vapour pressure of the ice, evaporation continues, the frozen mud surface cools, and  
 437 a wave of cooling propagates into the frozen mud. The bulk density of the mud changes  
 438 continuously throughout these stages as a function of the initial mass fractions of silicate and  
 439 water in the mud. Let the initial masses of water and silicate in a given sample of the mud be  
 440  $m_w$  and  $m_s$ , respectively, the volumes of water and solid be  $v_w$  and  $v_s$ , respectively, and the  
 441 corresponding densities be  $\rho_w$  and  $\rho_s$ . Let the bulk density of the mud be  $\beta$ . Then

442

$$443 \quad \beta = (m_w + m_s) / (v_w + v_s) = (m_w + m_s) / [(m_w / \rho_w) + (m_s / \rho_s)] \quad (1).$$

444

445 Expanding, collecting terms and simplifying:

446

$$447 \quad m_w / m_s = (\rho_w / \rho_s) [(\rho_s - \beta) / (\beta - \rho_w)] \quad (2).$$

448

449 We next find the mass of vapour,  $M_{vc}$ , that must be lost from the water to cool the  
 450 remaining water and silicate to any given lower temperature. Let the initial mud temperature be  
 451  $\theta_i$  and the final temperature be  $\theta_f$ . The heat  $H_v$  removed from the water by the formation of the  
 452 vapour is

453

$$454 \quad H_v = M_{vc} L_v \quad (3)$$

455

456 where  $L_v$  is the latent heat of vapourization,  $2.46 \times 10^6 \text{ J kg}^{-1}$ . During this cooling process, the  
457 liquid water mass decreases from its initial value  $m_w$  to a smaller final value  $m_f$ , where by  
458 definition

459

$$460 \quad m_f = m_w - M_{vc} \quad (4).$$

461

462 Thus, the average mass of water,  $m_a$ , during the cooling process is

463

$$464 \quad m_a = 0.5 (m_w + m_f) = 0.5 (m_w + m_w - M_{vc}) = (m_w - 0.5 M_{vc}) \quad (5).$$

465

466 As long as the specific heat of the water can be approximated as a constant, the heat the water  
467 loses while cooling is  $H_c$  where

468

$$469 \quad H_c = m_a C_w (\theta_i - \theta_f) \quad (6)$$

470

471 and  $C_w$  is the specific heat of water,  $4186 \text{ J kg}^{-1} \text{ K}^{-1}$ . The silicate mass  $m_s$  also cools, and loses  
472 an amount of heat equal to  $H_s$  where

473

$$474 \quad H_s = m_s C_s (\theta_i - \theta_f) \quad (7).$$

475

476 Here  $C_s$  is the specific heat of the silicate, say  $1000 \text{ J kg}^{-1} \text{ K}^{-1}$ . Equating the sum of  $H_c$  and  $H_s$   
477 to  $H_v$ ,

478

$$479 \quad (m_w - 0.5 M_{vc}) C_w (\theta_i - \theta_f) + m_s C_s (\theta_i - \theta_f) = M_{vc} H_v \quad (8)$$

480

481 and regrouping,

482

$$483 \quad M_{vc} [H_v + 0.5 C_w (\theta_i - \theta_f)] = (m_w C_w + m_s C_s) (\theta_i - \theta_f) \quad (9)$$

484

485 or

486

$$487 \quad M_{vc} / m_s = \{[(m_w / m_s) C_w + C_s] (\theta_i - \theta_f)\} / [H_v + 0.5 C_w (\theta_i - \theta_f)] \quad (10).$$

488

489 Using equation (2) for  $(m_w / m_s)$  we can also find  $(M_{vc} / m_s)$  as a function of the assumed value

490 of  $\rho_s$ . Finally, the ratio, R, of the mass of water converted to vapour to the initial water mass,

491 i.e.  $R = (M_{vc} / m_w)$ , is equal to  $[(M_{vc} / m_s) (m_s / m_w)]$  or more conveniently

492

$$493 \quad R = [(M_{vc} / m_s) / (m_w / m_s)] \quad (11).$$

494

495 The mass of water remaining in the mud after the cooling phase,  $m_f$ , is therefore

496

$$497 \quad m_f = (1 - R) m_w \quad (12).$$

498

499 The above equations apply between any pair of temperatures  $\theta_i$  and  $\theta_f$  until  $\theta_f$  becomes

500 equal to the freezing point,  $\theta_{fr}$ . After the freezing point is reached, the temperature remains

501 constant while liquid water continues to evaporate and the latent heat of vaporization is

502 extracted from the remaining water, progressively freezing into ice all of the water that is not

503 lost as vapour. The latent heat of vaporization in the 283-293 Kelvin range is  $2.46 \times 10^6 \text{ J kg}^{-1}$

504 and the latent heat of solidification is  $3.34 \times 10^5 \text{ J kg}^{-1}$ . The ratio of these is  $Q = (3.34 \times 10^5 /$

505  $2.46 \times 10^6) = 0.13577$ . Thus, to produce 1 kg of ice we would have to evaporate 0.13577 kg of

506 water into vapour from an initial total mass of 1.13577 kg of water. A fraction  $[Q/(1 + Q)]$  of  
 507 the water mass remaining after cooling must become vapour and a fraction  $[1/(1 + Q)]$  of the  
 508 water mass remaining after cooling becomes ice. The final ice mass,  $m_i$ , is

$$509$$

$$510 \quad m_i = [1/(1 + Q)] [(1 - R) m_w] \quad (13)$$

511  
 512 and the mass of water converted to vapour during the freezing phase is  $M_{vf}$  where

$$513$$

$$514 \quad M_{vf} = [Q/(1 + Q)] (1 - R) m_w \quad (14).$$

515  
 516 The total mass of vapour generated by the whole process is  $M_v = M_{vc} + M_{vf}$ .

517  
 518 As a result of the loss of vapour, the bulk density of the frozen mud will be different from  
 519 the density of the initial mixture. The ice has a density  $\rho_i$  of  $916.8 \text{ kg m}^{-3}$  so the mass  $m_i$  of ice  
 520 has a volume of  $v_i = (m_i / \rho_i)$ . The silicate volume is still  $v_s$  and so the final bulk density is  $\beta_f$   
 521 where

$$522$$

$$523 \quad \beta_f = (m_i + m_s) / (v_i + v_s) = (m_i + m_s) / [(m_i / \rho_i) + (m_s / \rho_s)] \quad (15).$$

524  
 525 Equation (12) gives  $(m_i / m_w)$  and equation (2) gives  $(m_w / m_s)$  so in terms of these,

$$526$$

$$527 \quad \beta_f = [(m_i / m_w) + (m_w / m_s)^{-1}] / \{[(m_i / m_w) / \rho_i] + [\rho_s (m_w / m_s)^{-1}]\} \quad (16).$$

528  
 529 The density,  $\rho_s$ , of the clay minerals in the experimental mud was  $\sim 2500 \text{ kg m}^{-3}$  and the bulk  
 530 density of the mud was  $\sim 1040 \text{ kg m}^{-3}$ , implying that the clay component formed  $\sim 6.5 \%$  of

531 the mud mass. The mud was released into ambient experimental chamber pressures in the  
532 range 650-700 Pa, and initial mud temperatures were up to  $\sim 275.5$  K. Taking account of the  
533 weight of the overlying mud and the experimental chamber pressure, the saturation vapour  
534 pressure of water, with values up to  $\sim 730$  Pa [48], would have been reached at depths up to  
535 5-6 mm in the experiments. The relative values of the specific heat and the latent heat of  
536 evaporation of water are such that while the mud was cooling from  $\sim 275.5$  K to its freezing  
537 point,  $\sim 0.34$  % of its water would have been lost, having a trivially small effect on its  
538 essentially Newtonian rheology. By the time subsequent vapour loss had frozen the  
539 remaining water,  $\sim 88$  % of the initial mass of water would have been converted to ice at the  
540 expense of losing  $\sim 12$  % of the initial water mass as vapour, leaving solid mud with a density  
541 of  $\sim 961$  kg m<sup>-3</sup>, slightly less dense than the original liquid mud. This should have produced  
542 a frozen crust, again of thickness 5-6 mm, beneath which the mud would have been partially  
543 liquid, as observed in the experiments. In similar scale flows under martian gravity, the  
544 thermodynamics of this process would have been the same, as it involves only heat transfer  
545 by conduction, but the thickness of the frozen outer crust would have been greater, 14-17  
546 mm, because the pressure in the mud depends on the acceleration due to gravity [49].

#### 547 **Data availability**

548 The movies, photos, pressure and temperature logs generated during and analysed during the  
549 current study that support our findings are available in the Zenodo repository with the identifier  
550 DOI: 10.5281/zenodo.3457148 (<https://doi.org/10.5281/zenodo.3457148>).

#### 551 **References**

552 [42] Platz, T., Byrne, P. K., Massironi, M. & Hiesinger, H. Volcanism and tectonism across the  
553 inner solar system: an overview. Geological Society, London, Special Publications 401,  
554 1–56 (2014).

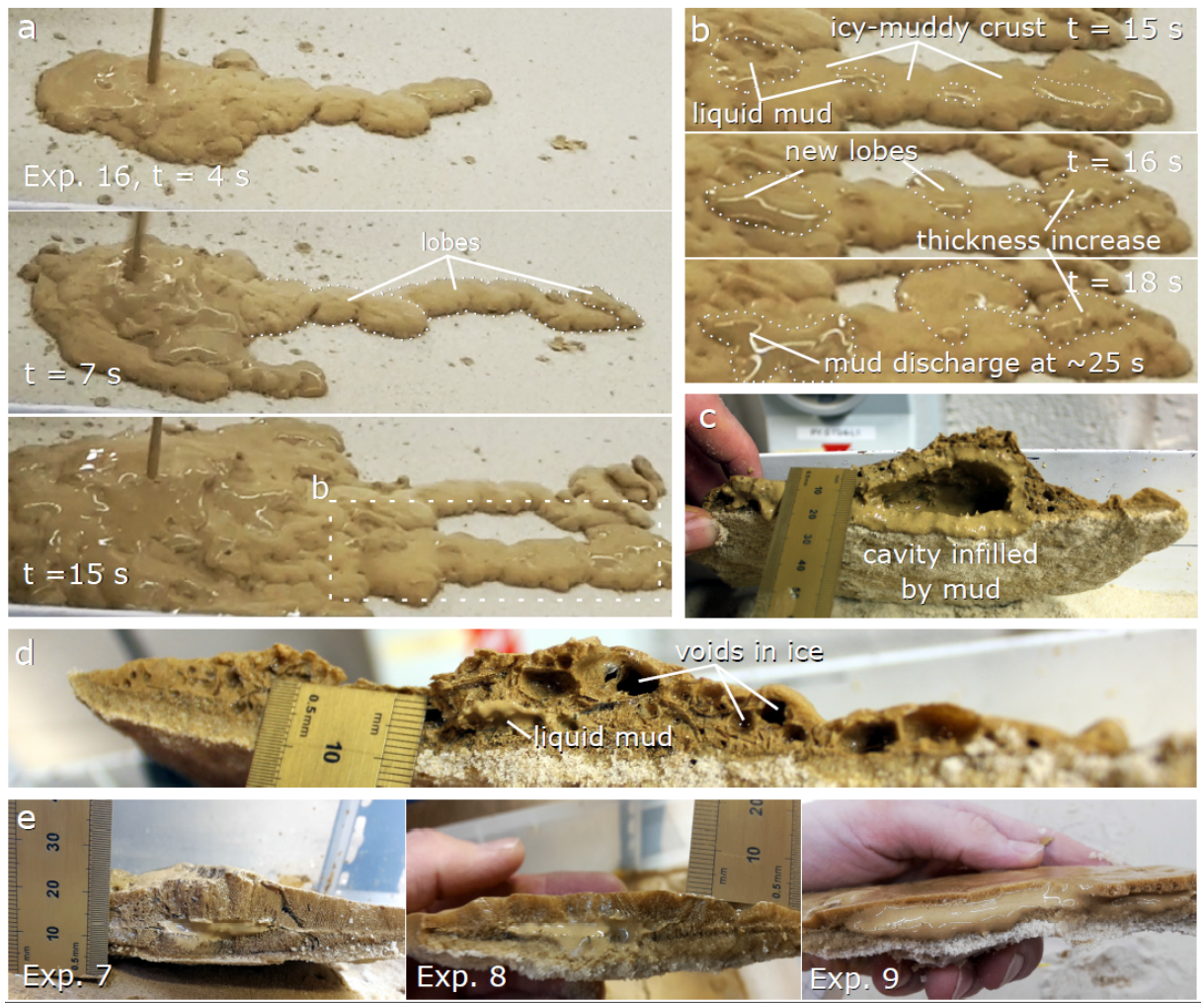
- 555 [43] Corradi, A. B., Manfredini T., Pellacani, G. C. & Pozzi, P. Deflocculation of Concentrated  
556 Aqueous Clay Suspensions with Sodium Polymethacrylates. *Journal of the American*  
557 *Ceramic Society* 77, 2, 509–513 (1994). [https://doi.org/10.1111/j.1151-](https://doi.org/10.1111/j.1151-2916.1994.tb07022.x)  
558 [2916.1994.tb07022.x](https://doi.org/10.1111/j.1151-2916.1994.tb07022.x)
- 559 [44] Clark, B. C. Implications of abundant hygroscopic minerals in the martian regolith. *Icarus*  
560 34, 645–665 (1978). [https://doi.org/10.1016/0019-1035\(78\)90052-0](https://doi.org/10.1016/0019-1035(78)90052-0)
- 561 [45] Vaniman, D. T. et al. Magnesium sulphate salts and the history of water on Mars. *Nature*  
562 431, 663–665 (2004). <https://doi.org/10.1038/nature02973>
- 563 [46] Hecht, M. H., et al. Detection of perchlorate and the soluble chemistry of martian soil at  
564 the Phoenix lander site. *Science* 325, 64–67 (2009).  
565 <https://doi.org/10.1126/science.1172466>
- 566 [47] Westoby, M. J., Brasington, J., Glasser, N. F., Hambrey, M. J. & Reynolds, J. M.  
567 ‘Structure-from-motion’ photogrammetry: a low-cost, effective tool for geoscience  
568 applications. *Geomorphology* 179, 300–314 (2012).  
569 <https://doi.org/10.1016/j.geomorph.2012.08.021>
- 570 [48] Lide, D. R. (ed.). *CRC Handbook of Chemistry and Physics* (85th edition, CRC Press,  
571 Boca Raton, Florida, 2004).
- 572 [49] Pedersen, G. B. M. Frozen Martian lahars? Evaluation of morphology, degradation and  
573 geologic development in the Utopia-Elysium transition zone. *Planetary and Space*  
574 *Science* 85, 59–77 (2013). <https://doi.org/10.1016/j.pss.2013.05.020>



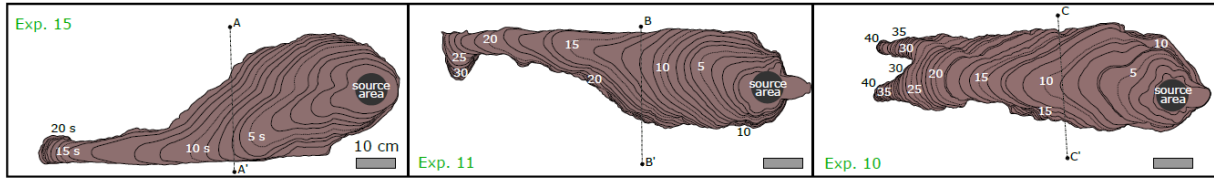
575



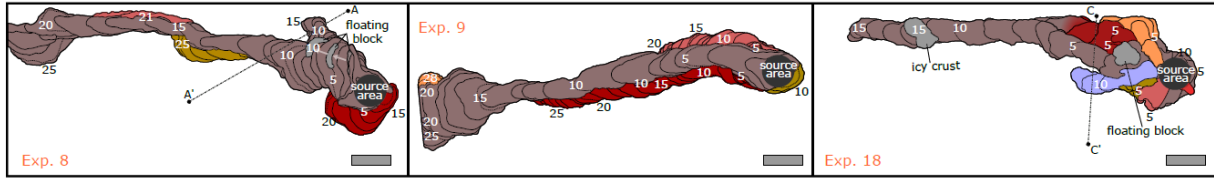
576



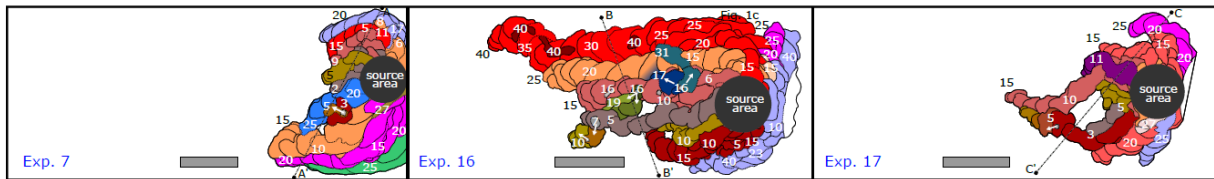
**a) ambient pressure, variable release rates**



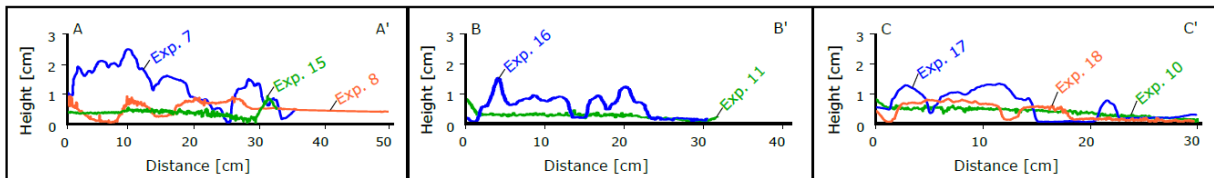
**b) pressure ~7 mbar, 'high' release rates**



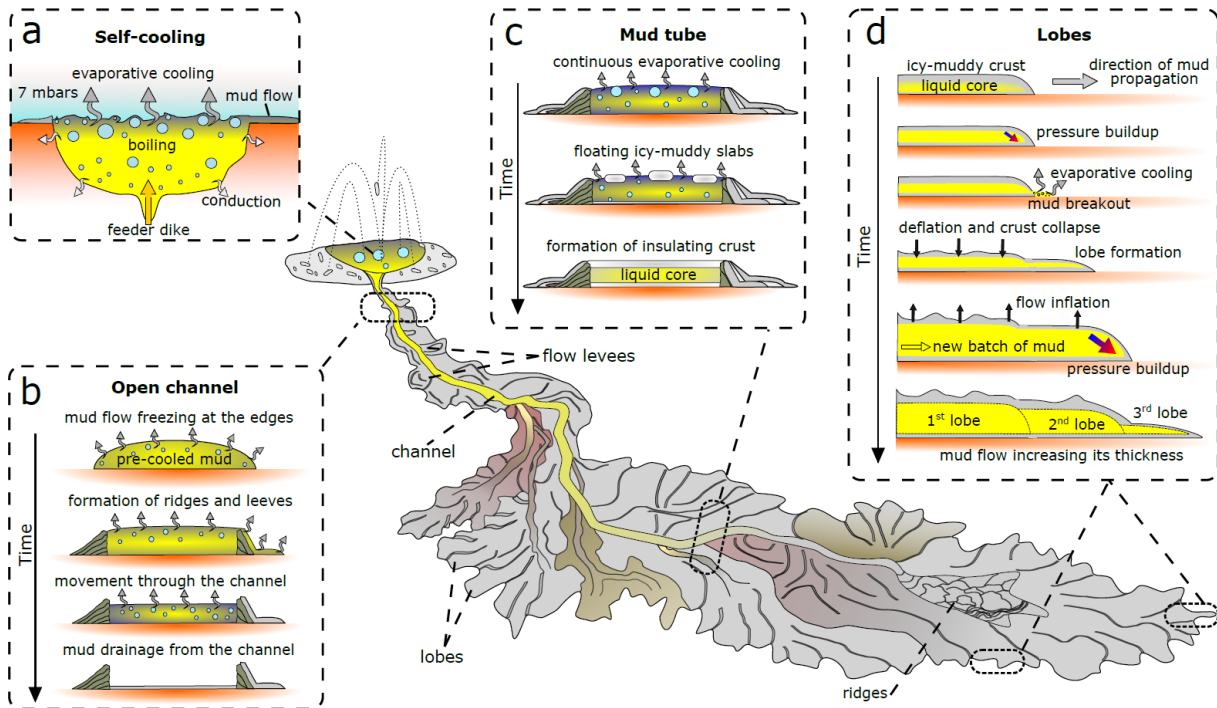
**c) pressure ~7 mbar, 'low' release rates**



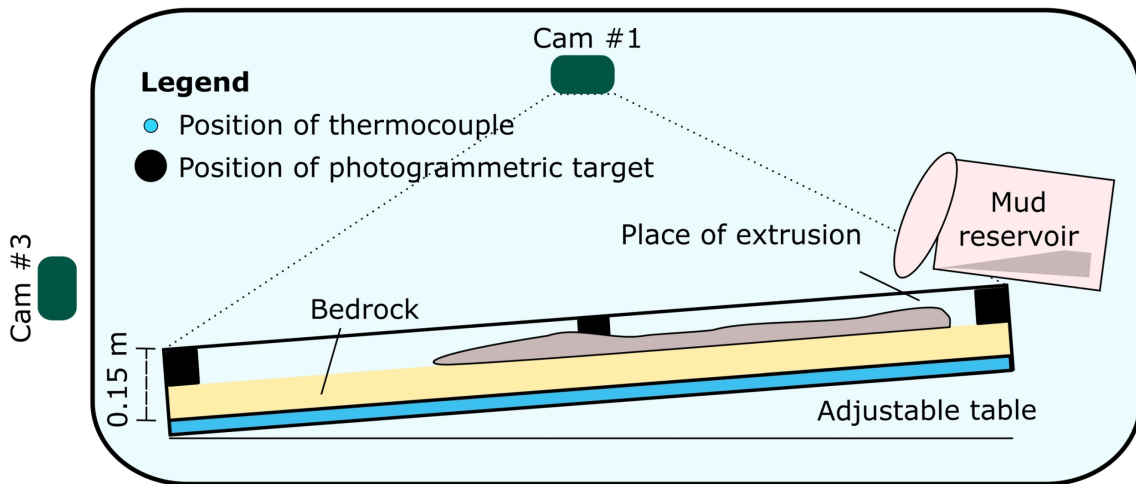
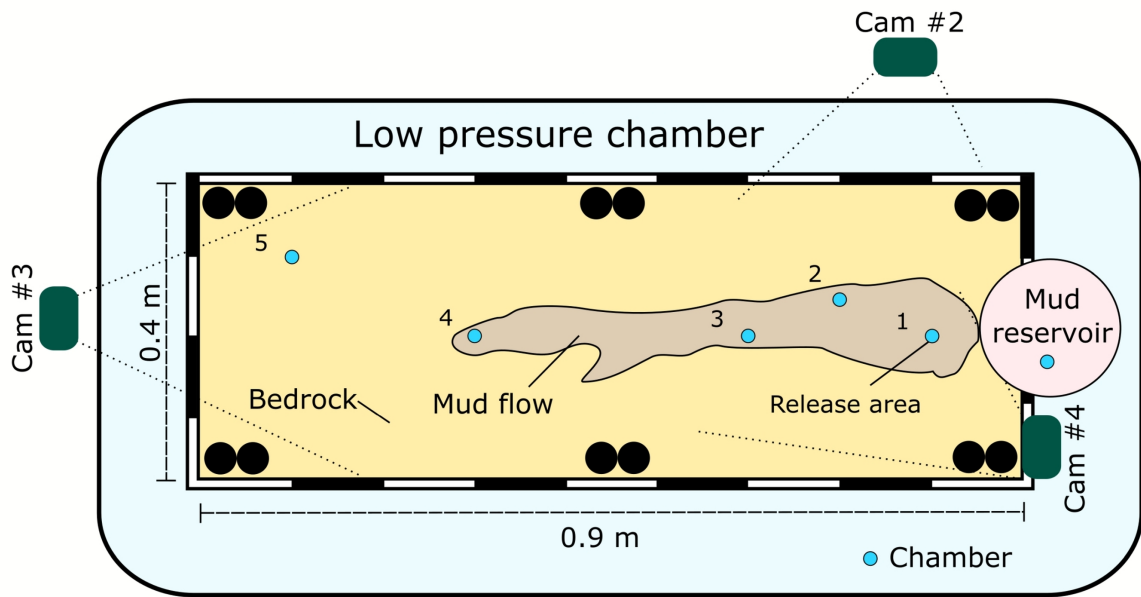
**d) topography**



577



578



Exp #	Pressure range [mbar]	Inclination [°]	Release time* [s]	Surface T** [°K]	Mud T*** [°K]	Type of surface	Salinity****
5	6.55 - 7.33	5	15	265	294	sand	D.I. water
6	7.16 - 7.66	5	26	264	292	sand	tap water
7	6.43 - 7.02	5	27	258	296	sand	saline water
8	7.11 - 7.37	5	25	261	294	sand	saline water
9	7.09 - 7.63	5	27	262	294	sand	saline water
10	1000	5	21	258	290	sand	saline water
11	1000	5	19	264	274	sand	saline water
15	1000	5	15	258	293	sand	saline water
16	6.32 - 6.54	5	46	256	290	sand	saline water
17	6.57 - 6.94	5	34	252	278	sand	saline water
18	6.37 - 6.58	5	15	260	290	sand	saline water
19	6.06 - 6.81	10	35	258	286	sand	saline water
21	6.55 - 6.77	10	34	253	293	sand	saline water
22	7.08 - 7.36	10	37	254	294	sand	saline water
23	6.43 - 6.97	5	40	265	293	plastic plate	saline water
24	6.66 - 7.11	5	28	254	295	plastic plate	saline water
29	6.55 - 7.08	5	40	259	295	plastic plate	saline water
34	5.29 - 6.55	5	failed exp.	259	297	plastic plate	saline water
41	1000	5	42	244	295	plastic plate	saline water
49	1000	5	34	247	290	plastic plate	saline water
54	1000	5	34	249	277	plastic plate	saline water

\* Time period over which the mud was poured from the container

\*\* Temperature of the surface before the release of the mud from the flipping container

\*\*\* Temperature of the mud within the container before the pressure drop

\*\*\*\* Saline water refers to a mixture of water that contains 0.5% w/w dissolved magnesium sulphate (MgSO<sub>4</sub>)